

Super-resolution reconstruction for underwater imaging

YUZHANG CHEN¹, WEI LI^{1*}, MIN XIA¹, QING LI², KECHENG YANG¹

¹Wuhan National Laboratory for Optoelectronics, College of Optoelectronic Science and Engineering, Huazhong University of Science and Technology, Wuhan 430074, China

²Department of Information Science and Technology, Huazhong University of Science and Technology, Wuchang Branch, Wuhan 430074, China

*Corresponding author: aliceliwei@gmail.com

In order to enhance the visual quality of images obtained by underwater imaging systems, super resolution (SR) reconstruction is introduced, including single-frame and multi-frame SR algorithms. Experimental images from a range-gated pulsed laser imaging system are processed by SR algorithms, results are evaluated and compared by blind, objective quality metrics. Results show that the image quality of underwater imaging can be effectively enhanced if the appropriate SR reconstruction algorithm is chosen.

Keywords: super-resolution reconstruction, range-gated, quality metrics.

1. Introduction

Underwater imaging is widely used in ocean exploration and other fields, however, due to absorption and scattering effects from the environment, serious degradation exists in underwater images, mainly in the form of noise, blur, *etc.* Resolution is an important parameter for image evaluation, therefore improving the image quality of underwater imaging, especially in terms of human vision, largely depends on the enhancement of spatial resolution.

Improving resolution of underwater imaging can be conducted from two perspectives. From the hardware perspective, appropriately increasing the intensity of laser, enhancing detection rates of sensor and reducing error rate are effective ways; however, these will undoubtedly increase the system cost. Under a certain hardware condition, processing by software has become a crucial step. As for the software perspective, image processing can effectively eliminate Gaussian, speckle noise, and improve image clarity, such as image denoising, enhancement and restoration algorithms. But no matter how efficacious these algorithms are, resolution is still limited by hardware conditions.

Image super-resolution reconstruction which has been increasingly popular in recent years offers the possibility of improving image resolution beyond the hardware limitations. It has been widely used ever since TSAI and HUANG [1] proposed the concept in 1984. It refers to achieving high-resolution (HR) enlargements of pixel-based images from one or multiple low-resolution (LR) images [2] using the complementary information between image sequences. Super-resolution (SR) reconstruction consists of three steps: registration, fusion, and reconstruction [3]. Image registration transfers LR images into non-uniform samples, which then will be processed by image fusion using interpolation or other methods to HR images.

Super-resolution reconstruction can be divided into categories according to frequency domain and spatial domain. Methods in the frequency domain improve resolution by eliminating aliasing, such as the recursive least squares method proposed by BOSE in 1990 [4]. However, the application of frequency domain based methods is limited by linear space invariance, which makes space domain based methods become hot research topics. Methods in the space domain improve resolution by combining the motion model with interpolation and iteration. Typical methods such as interpolation, iterative back projection (IBP) [5], projection onto convex sets (POCS) [6], mixed MAP/POCS method, as well as adaptive filtering, Kalman filtering methods are widely used.

The presented effort applies several super-resolution reconstruction algorithms to underwater range-gated imaging. The validity of the algorithms is verified by image evaluation.

2. Theory

2.1. Single frame super-resolution reconstruction

The main approach of single frame super-resolution reconstruction is interpolation, by which the discrete image is converted into continuous data sets, and then to a high-resolution image through resampling. Standard pixel interpolation methods such as pixel replication and cubic-spline interpolation [7] are widely used in image enhancement. The main idea of pixel replication is inserting pixels with values of or between those of known pixels. Cubic-spline interpolation belongs to higher order interpolation, which utilizes an approximate sampling function for interpolation, with imposing boundary conditions; as a result, the interpolated result will have better smoothness and visual effect.

The low-pass effect of the interpolation operator can result in blocking artifacts and edge degradation. Wavelet transform with the features of multi-resolution and time-frequency localization can be an effective tool to eliminate this degradation by processing an image in high and low frequency domains separately. In order to avoid the unmatched high and low frequency and loss of information caused by direct use of original image for inverse wavelet transform, high frequency coefficients for inverse wavelet transform are derived from bilinear interpolation, while low frequency

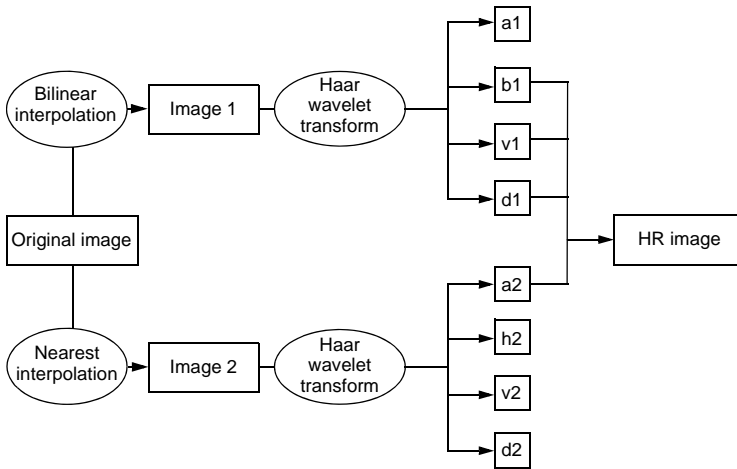


Fig. 1. Block diagram of wavelet-based interpolation algorithm.

coefficients are obtained from nearest interpolation. Figure 1 shows the algorithm of improved wavelet-based interpolation, in which blocks with a_i denote low frequency coefficient; while the ones with h_i , v_i and d_i represent high frequency coefficients of horizontal, vertical and diagonal directions, respectively.

The Papoulis–Gerchberg (PG) method, proposed and studied independently by PAPOULIS [8] and GERCHBERG [9], is an extrapolation method based on the frequency domain. The theory of the PG method has been studied by many researchers recently [10] and some of them proposed improved versions [11]. The main idea of the PG method is extrapolation of a band limited signal from only a part of the original signal by iterating terminated by error energy reduction. The extrapolation in the n -th iteration (frequency domain) can be expressed as:

$$F_n(\omega) = G_{n-1}(\omega)p_\sigma(\omega), \quad p_\sigma(\omega) = \begin{cases} 1, & |\omega| < \sigma \\ 0, & |\omega| > \sigma \end{cases} \quad (1)$$

$g(t)$ is the time domain expression of $G(w)$ and $g(t)$ denotes a finite segment of $f(t)$ with a cut-off frequency of σ :

$$g(t) = f(t)p_T(t), \quad p_T(t) = \begin{cases} 1, & |t| < T \\ 0, & |t| > T \end{cases} \quad (2)$$

In the iteration process, the energy reduction error between the signals of the n -th iteration and the $(n + 1)$ -th iteration is reduced, thus, the extrapolated signal can approach the desired signal with sufficient iterations. The iteration can be expressed by:

$$g_n(t) = f_n(t) + [f(t) - f_n(t)]p_T(t) = \begin{cases} g(t), & |t| \leq T \\ f_n(t), & |t| > T \end{cases} \quad (3)$$

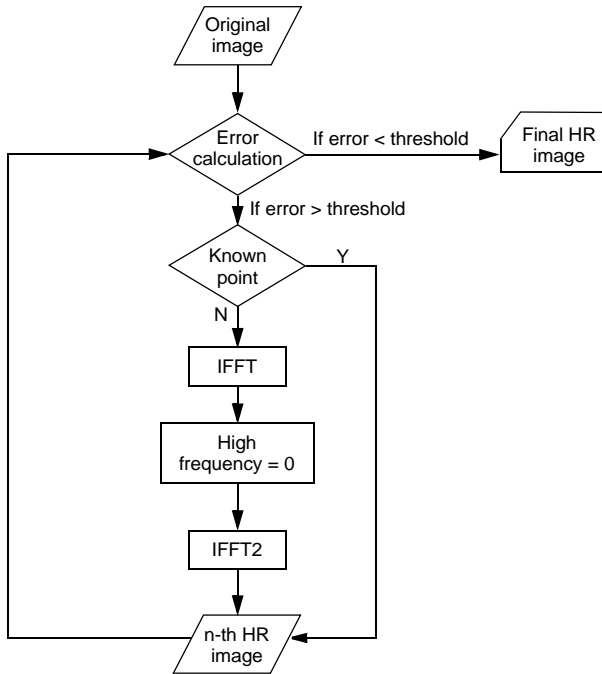


Fig. 2. Flowchart of an algorithm based on the Papoulis–Gerchberg method.

Figure 2 shows a flowchart of the PG method, in which the known points are pixels from the original image, while others are extrapolated pixels. The iteration is terminated by the calculation of energy reduction error between reconstructed images.

2.2. Multi-frame super-resolution reconstruction

Images captured by the same sensor in time series can be used for multi-frame image super-resolution reconstruction. Image registration is an important step before multi-frame SR reconstruction. It is a mapping operation between two images spatially, which can also be divided into two types according to spatial and frequency domains. Methods in frequency domain use the phase correlation to estimate the motion parameters and reduce the aliasing error [12], while the spatial motion model is used by methods in the spatial domain [13]. Keren image registration [14] is used for underwater imagery for its common evaluation of accuracy and robustness. The algorithm is based on a rigid body transformation model:

$$g(x, y) = f(x \cos \theta - y \sin \theta + a, y \cos \theta + x \sin \theta + b) \quad (4)$$

which has three parameters: a – horizontal shift, b – vertical shift, and θ – rotation angle. Then, based on the Taylor series transform, error function between $g(x, y)$ and

$f(x, y)$ can be obtained. In order to minimize the error function, partial derivatives are used; then, SR images can be obtained by interpolation, *etc.*

The iterative back-projection (IBP) method is proposed by IRANI and PELEG [5]. It performs projection and back-projection iteratively with the convergence of error projected onto the HR image grid. The traditional IBP method can induce various degrees of ringing artifacts. An improved IBP method [15] is applied, which can be expressed by the mathematical description

$$f^{n+1} = f^n - \lambda \left(\sum_{i=1}^P H(g_i^n - g_i) - (\Delta f_i^n - \Delta f_c) \right) \tag{5}$$

where f^{n+1} denotes the SR image resulting from the $(n + 1)$ -th iteration, f^n denotes SR image in the n -th iteration, while g_i^n denotes the LR image; λ is the gradient step, Δ is the Laplace operator, $(\Delta f_i^n - \Delta f_c)$ can represent the ringing artifacts, H is the blurring operator which can be derived from point spread function (PSF) of imaging systems.

Projection onto convex sets (POCS) proposed by Stark and Oskou is one of the spatial-domain-based SRR algorithms with its flexibility of incorporating prior information such as the PSF of the imaging system. The POCS method can be described as an iterative equation:

$$f^{n+1} = P \left[f^n + \sum_{i=1}^k \lambda P(g_i - Hf_i) \right] \tag{6}$$

where k denotes the number of limit sets, P denotes the projection operator, f^{n+1} and f^n denote the SR image resulting from the $(n + 1)$ -th iteration and n -th iteration, g represents low-resolution image, λ represents relaxed operator, and H is the blurring operator which can be derived from PSF of imaging systems. As for underwater imaging systems, the PSF of the system can be derived from Wells' small angle approximation [16] which can be described as:

$$h(\theta, R) = 2\pi \int J_0(2\pi\theta\varphi) H(\varphi, R) \varphi d\varphi \tag{7}$$

$$H(\varphi, R) = \exp \left[-cR + bR \frac{1 - \exp(-2\pi\theta_0\varphi)}{2\pi\theta_0\varphi} \right] \tag{8}$$

where $H(\varphi, R)$ denotes the modulation transfer function (MTF) of the imaging system, and φ denotes the spatial frequency, R is the imaging distance, c and b represent total attenuation and scattering coefficient, respectively, θ_0 is referred to the median scattering angle for single scattering and cR means optical length.

The robust super-resolution is a relatively new method proposed in 2001 [17]. The main idea of this method has some resemblance to that of IBP method. The iterative equation of this method is:

$$f^{n+1} = f^n + \lambda \nabla L(f) \quad (9)$$

$$\nabla L(f) = n \cdot \text{median}\{B_k\}_{k=1}^n \quad (10)$$

where λ is the scale factor of the gradient step size, f^{n+1} and f^n denote SR images resulting from the $(n+1)$ -th iteration and n -th iteration, respectively, B_k represents the back-projected difference image, $\nabla L(f)$ is equal to a scaled pixel-wise median with the purpose of introducing robustness into super-resolution. A median can approximate the mean quite accurately for a symmetric distribution, given a sufficient set of samples. In case of distant outliers, the median is much more robust than the mean.

2.3. Image evaluation

In order to evaluate the performance of SR methods applied in underwater imaging, metrics for measuring visual quality are needed. Image quality metrics can be divided into subjective and objective ones [18]. Subjective metrics need manpower and time, while objective metrics are widely used, which can also be divided into two types depending on the demand of ideal image. As for underwater images, no reference image can be provided, thus, blind, objective image quality metrics are needed.

The metrics chosen are gray mean grads (GMG), Laplacian sum (LS) proposed by SHEIKH and BOVIK [19]. GMG and LS can effectively reflect the clarity and edge profile of an image as one can see from mathematical expressions:

$$\text{GMG} = \frac{\sum_{i=1}^{M-1} \sum_{j=1}^{N-1} \sqrt{\frac{[g(x, y+1) - g(x, y)]^2 + [g(x+1, y) - g(x, y)]^2}{2}}}{(M-1)(N-1)} \quad (11)$$

$$\text{LS} = \frac{\sum_{i=1}^{M-1} \sum_{j=1}^{N-1} |X|}{(M-2)(N-2)} \quad (12)$$

where $X = 8g(x, y) - g(x, y-1) - g(x-1, y) - g(x+1, y) - g(x, y+1) - g(x-1, y-1) - g(x-1, y+1) - g(x+1, y-1) - g(x+1, y+1)$.

Information capacity [20] can also be used, which is defined as:

$$C(d, \theta) = \log_2 \left\{ 1 + \sum_w \frac{\log [p(i, j, d, \theta)]}{\log [\max(p(i, j, d, \theta))]} \right\} \tag{13}$$

where $p(i, j, d, \theta)$ describes the relativity between pixels which have gray levels of i and j , distance of d , and direction of θ . As can be seen from the above, the GMG, LS and information capacity of better images are higher than those of degraded ones.

3. Experimental setup

The test images for image super-resolution methods described above were obtained from a range-gated imaging system we set up, which consists of a 532-nm pulsed laser and an ICCD with programmable timing generator as external trigger controller. The imaging target is a stripe resolution board covered by regularly distributed white

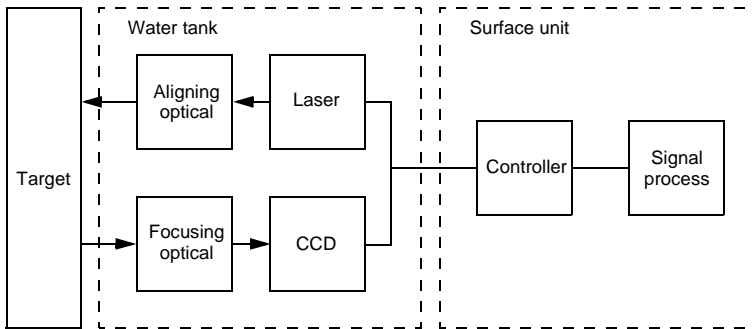


Fig. 3. Block diagram of range-gated imaging system.

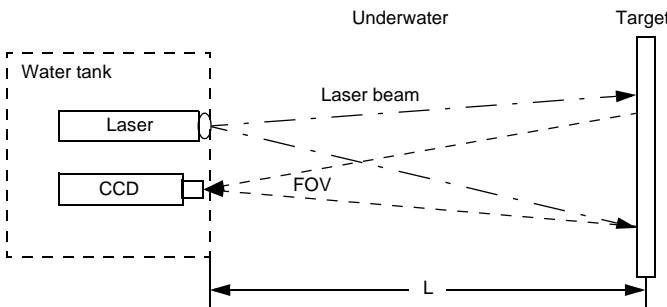


Fig. 4. Schematic diagram of range-gated imaging system.

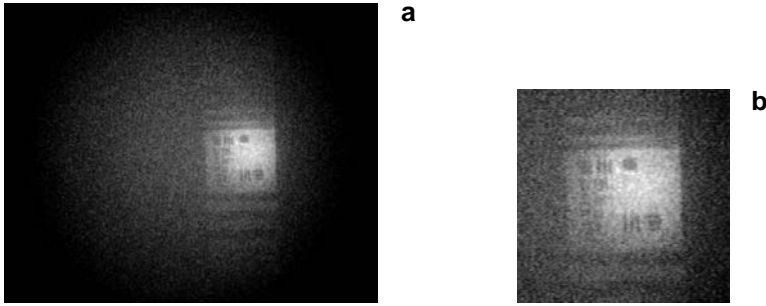


Fig. 5. Sample image of original size (a), and region of interest (b).

stripes with a black background. Figures 3 and 4 show the block and schematic diagrams of the experimental system.

Experiments were conducted in a boat pond with a length of 200 m. The target was located at a distance of 35 m from the laser and the CCD. The angle of field of view (FOV) is about 4 degrees. The attenuation coefficient of the water and the scattering albedo were measured as $c = 0.159 \text{ m}^{-1}$ and $\omega = 0.85$. 10 frames of the test video sequences collected by CCD are extracted for SR reconstruction tests. A sample image is shown in Fig. 5 (original size 720×576 pixels, region of interest 256×256 pixels).

Figure 5b is used for a single frame image super-resolution reconstruction, while the whole image sets are used for multi-frame super-resolution reconstruction

3.1. Image preprocessing

Characteristic noises appearing in CCD images have been considered to be the most harmful phenomenon in imaging systems [21]. So, image noise should be analyzed and filtered before SR reconstruction in order to avoid the amplification of noise. Fixed pattern noise (FPN) and Gaussian noise are the two types of noise generally appearing in images obtained by CCD. The former can be easily eliminated for its fixed feature, while Gaussian noise needs to be processed by denoising algorithms. The Gaussian filter is a typical denoising tool; however, its performance weakens when the signal to noise ratio of image is too low. Wavelet-based denoising scheme can keep a certain balance between denoising and keeping details, while the bilateral filter [22] is a denoising filter based on Gaussian filtering, the weight coefficient of which is composed by the low pass filter and brightness information; thus, it can eliminate noise and keep edge details simultaneously. Its mathematical expression is:

$$g(x) = k^{-1}(x) \int_{-\infty}^{\infty} \int_{-\infty}^{\infty} f(\varepsilon) c(\varepsilon, x) s(f(\varepsilon), f(x)) d\varepsilon \quad (14)$$

where $k(x) = \int_{-\infty}^{\infty} \int_{-\infty}^{\infty} c(\varepsilon, x) s(f(\varepsilon), f(x)) d\varepsilon$, $c(\varepsilon, x) = \exp\left[-\frac{d(\varepsilon, x)^2}{2\sigma_d^2}\right]$ represents

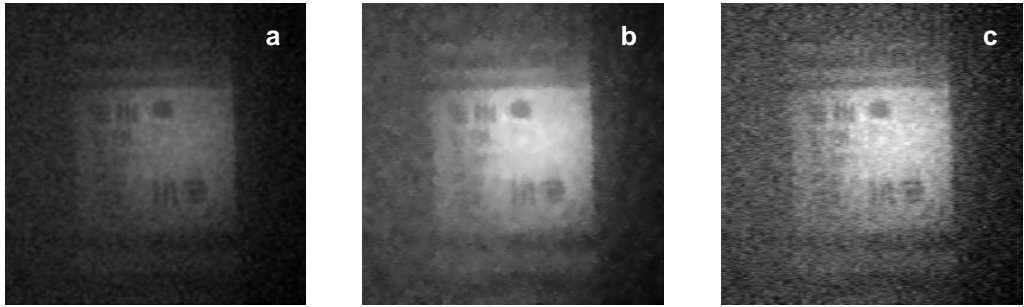


Fig. 6. Denoising results (size: 256×256) of Gaussian filter (a), bilateral filter (b), wavelet filter (c).

Table 1. Comparison of evaluation metrics of denoising results.

	Original	Gaussian	Bilateral	Wavelet
GMG	2677964	2024402	2948232	2744921
LS	13828584	7126142	22119831	18321959
Cinfo	0.0227	0.0294	0.8750	0.0805

the spatial proximity function, $s(f(\epsilon), f(x)) = \exp\left[-\frac{\delta(f(\epsilon), f(x))^2}{2\sigma_r^2}\right]$ denotes

the gray similarity function, σ_d and σ_r denote the standard deviation of Gaussian function. Figure 6 shows the denoising results. GMG, LS and information capacity of the original image and denoising results are shown in Tab. 1.

It can be easily seen even from the resultant images that bilateral filtering performs much better than Gaussian and wavelet filters. As a result, bilateral denoising is chosen for the preprocess of SR reconstruction.

3.2. Super-resolution reconstruction

The results of single frame super-resolution reconstruction methods are shown in Fig. 7. Table 2 shows GMG, LS and information capacity of the original image and reconstruction results.

We can see that the performance of interpolation algorithms is not satisfactory as expected, only improved wavelet-based interpolation and PG method can offer relatively better results. Traditional interpolation methods failed in improving image quality due to its operation of creating non-existing pixels that blurs the boundaries of black and white, which degrades the boundaries of black and white stripes. Improved wavelet-based interpolation operates in the wavelet domain and values of interpolated pixels are not simply linear transformation of existing pixels, so that it can preserve the edge information. The PG method is an extrapolation method which operates due to energy error reduction, and can also avoid blurring.

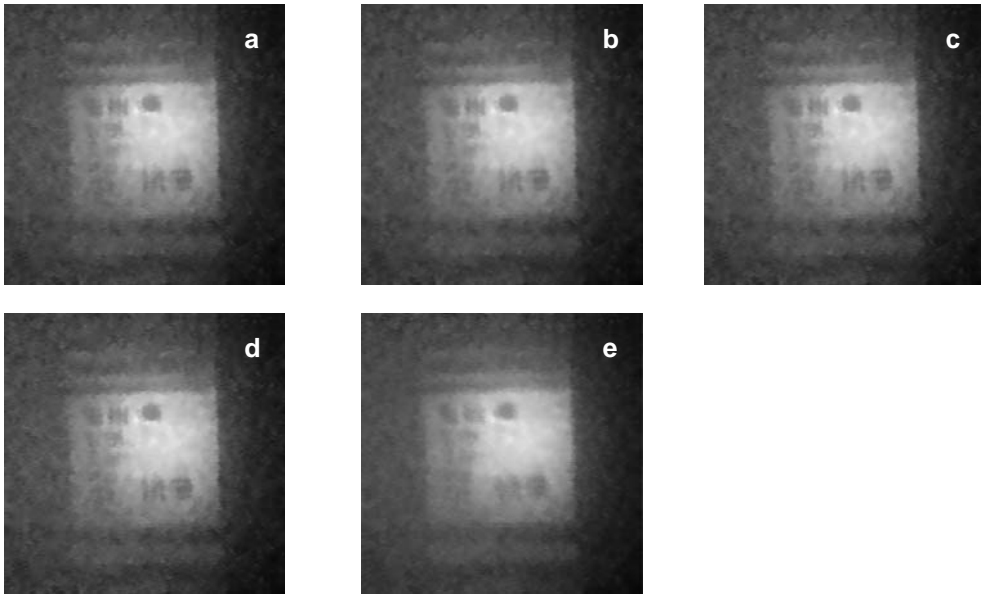


Fig. 7. SR reconstruction results (size: 512×512) of nearest interpolation (a), bilinear interpolation (b), cubic-spline interpolation (c), wavelet-based interpolation (d), and Papoulis–Gerchberg method (e).

Table 2. Comparison of evaluation metrics of single-frame reconstruction results.

	Nearest	Bilinear	Cubic	Wavelet	PG
GMG	2201032	1482923	1867139	2281622	6928387
LS	12038072	4655161	6317201	21489991	23174544
Cinfo	0.0227	0.0023	0.0059	0.0247	0.0280

Figure 8 shows the results of multi-frame super-resolution reconstruction methods. Values of evaluation metrics for Fig. 8 are shown in Tab. 3, in which the a , b and θ are the shift values and rotated angle calculated by Keren image registration.

It can be seen that multi-frame SR algorithms perform better than single-frame SR algorithms, which is not difficult to think of because multi-frame images contain more

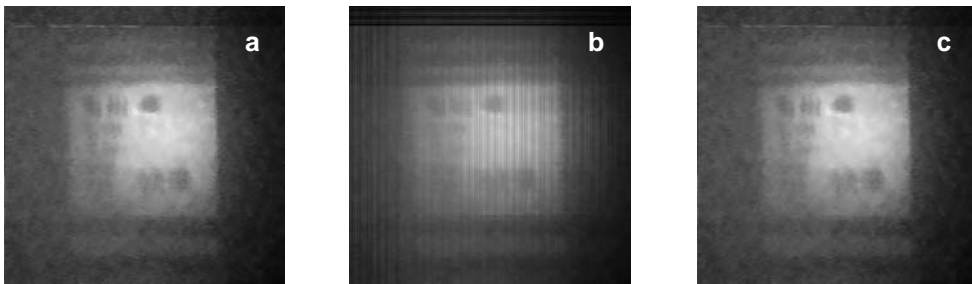


Fig. 8. SR reconstruction (size: 512×512) results of IBP (a), POCS (b), and robust SR (c).

Table 3. Comparison of evaluation metrics of multi-frame reconstruction results.

	a	b	θ	IBP	POCS	Robust SR
GMG				16551701	7660501	12697107
LS	1.06178	19.5214	1.7984	92018103	37496951	67565361
Cinfo				0.1002	0.0240	0.0505

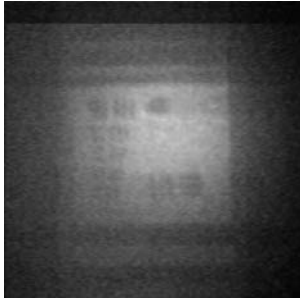


Fig. 9. SR reconstruction results (size: 512×512) of POCS method with estimated PSF.

Table 4. Comparison of evaluation metrics of traditional POCS and that with PSF.

	POCS	PSF-based POCS
GMG	7660501	20081956
LS	37496951	121399379
Cinfo	0.0240	0.2361

information than one single image. However, owing to the steep cut-off frequency, resultant HR images have some ringing artifacts which can be obviously seen from Fig. 8b. As a result, some kind of regularization is needed to decrease the ringing drawbacks.

The reconstruction results of the POCS method with regularization by the PSF of the imaging system is shown in Fig. 9, the parameters used to estimate the PSF are from the physical properties of experimental facilities including the diffraction limit of sensors. The image quality of Fig. 9 is compared with that of the traditional POCS method in Tab. 4.

From Table 4, we can clearly see an enormous increase in information capacity when a PSF is used. This is due to the prior information the PSF contains, in which the diffraction limit of sensors is the most useful one. As a result, it can be concluded that the merge of prior information can substantially enhance the performance of SR reconstruction, which can achieve the best result currently.

4. Conclusions

The presented effort introduces image super-resolution reconstruction to underwater imaging. Varied SR reconstruction algorithms are applied to an underwater range-gated pulsed laser imaging system. Experimental results show that multi-frame SR recon-

struction algorithms perform better than single-frame SR algorithms, the deployment of prior knowledge can enhance the performance of traditional SR algorithms such as POCS. Further research will be conducted from two aspects, the research for a better estimated PSF for SR algorithm, and applications of other SR algorithms.

References

- [1] TSAI R.Y., HUANG T.S., *Multi-frame image restoration and registration*, [In] *Advances in Computer Vision and Image Processing*, Vol. 1, No. 2, JAI Press Inc., Greenwich, CT, 1984, pp. 317–339.
- [2] SUNG CHEOL PARK, MIN KYU PARK, MOON GI KANG, *Super-resolution image reconstruction: A technical overview*, IEEE Signal Processing Magazine **20**(3), 2003, pp. 21–36.
- [3] ZHAO W., SAWHNEY H., HANSEN M., SAMARASEKERA S., *Super-fusion: A super-resolution method based on fusion*, Proceedings of 16th International Conference on Pattern Recognition, Vol. 2, 2002, pp. 269–272.
- [4] BOSE N.K., *Recursive reconstruction of images from noisy and blurred multiframe*, Realization and Modelling in System Theory, Proceedings of the International Symposium MTNS-89, Vol. 1, 1989, pp. 319–24.
- [5] IRANI M., PELEG S., *Improving resolution by image registration*, CVGIP: Graphical Models and Image Processing **53**(3), 1991, pp. 231–239.
- [6] PATTI A.J., SEZAN M.I., MURAT TEKALP A., *Superresolution video reconstruction with arbitrary sampling lattices and nonzero aperture time*, IEEE Transactions on Image Processing **6**(8), 1997, pp. 1064–1076.
- [7] BLU T., THEVENAZ P., UNSER M., *Linear interpolation revitalized*, IEEE Transactions on Image Processing **13**(5), 2004, pp. 710–719.
- [8] PAPOULIS A., *A new algorithm in spectral analysis and band-limited extrapolation*, IEEE Transactions on Circuits and Systems **CAS-22**(9), 1975, pp. 735–742.
- [9] GERCHBERG R.W., *Super-resolution through error energy reduction*, Optica Acta **21**(9), 1974, pp. 709–720.
- [10] FERREIRA P.J.S.G., *Interpolation and the discrete Papoulis–Gerchberg algorithm*, IEEE Transactions on Signal Processing **42**(10), 1994, pp. 2596–2606.
- [11] CHATTERJEE P., MUKHERJEE S., CHAUDHURI S., SEETHARAMAN G., *Application of Papoulis–Gerchberg method in image super-resolution and inpainting*, Computer Journal **52**(1), 2009, pp. 80–89.
- [12] VANDEWALLE P., SUSSTRUNK S., VETTERLI M., *A frequency domain approach to registration of aliased images with application to super-resolution*, EURASIP Journal on Applied Signal Processing, No. 10, 2006, p. 14.
- [13] BERGEN J.R., ANANDAN P., HANNA K.J., *Hierarchical model-based motion estimation*, Second European Conference on Computer Vision Proceedings, Computer Vision – ECCV’92, pp. 237–252.
- [14] KEREN D., PELEG S., BRADA R., *Image sequence enhancement using sub-pixel displacements*, Proceedings CVPR’88: The Computer Society Conference on Computer Vision and Pattern Recognition, pp. 742–746.
- [15] HAIYING S., XIAOHAI H., WEILONG C., *An improved iterative back-projection algorithm for video super-resolution reconstruction*, Proceedings 2010 Symposium on Photonics and Optoelectronics (SOPO 2010), p. 4.
- [16] FAN F., KECHENG Y., BO F., *Application of blind deconvolution approach with image quality metric in underwater image restoration*, 2010 International Conference on Image Analysis and Signal Processing (IASP 2010), pp. 236–239.

- [17] ZOMET A., RAV-ACHA A., PELEG S., *Robust super-resolution*, Proceedings of the 2001 IEEE Computer Society Conference on Computer Vision and Pattern Recognition, CVPR 2001, Vol. 1, pp. 645–650.
- [18] HOU W., WEIDEMANN A.D., *Objectively assessing underwater image quality for the purpose of automated restoration*, Proceedings of SPIE **6575**, 2007, p. 65750Q.
- [19] SHEIKH H.R., BOVIK A.C., *Image information and visual quality*, IEEE Transactions on Image Processing **15**(2), 2006, pp. 430–444.
- [20] HONGWEI H., XIAOHUI Z., WEILONG G., *Performance evaluation of underwater range-gated viewing based on image quality metric*, Proceedings of the 2009 9th International Conference on Electronic Measurement Instruments (ICEMI 2009), pp. 4–441.
- [21] FARAJI H., MACLEAN W.J., *CCD noise removal in digital images*, IEEE Transactions on Image Processing **15**(9), 2006, pp. 2676–2685.
- [22] MING Z., GUNTURK B., *A new image denoising method based on the bilateral filter*, ICASSP 2008, IEEE International Conference on Acoustic, Speech and Signal Processes, 2008, pp. 929–932.

*Received December 16, 2010
in revised form May 1, 2011*